Earth and Planetary Science Letters 399 (2014) 86–91

Contents lists available at ScienceDirect

Earth and Planetary Science Letters

www.elsevier.com/locate/epsl

The effect of Fe spin crossovers on its partitioning behavior and oxidation state in a pyrolitic Earth's lower mantle system

Clemens Prescher [a,*,1], Falko Langenhorst [b], Leonid S. Dubrovinsky [a], Vitali B. Prakapenka [c], Nobuyoshi Miyajima [a]

[a] Bayerisches Geoinstitut, University of Bayreuth, 95440 Bayreuth, Germany
[b] Institute for Geosciences, Mineralogy Dept., University of Jena, 07745 Jena, Germany
[c] Center for Advanced Radiation Sources, University of Chicago, Chicago, IL 60439, USA

ARTICLE INFO

Article history:
Received 20 July 2013
Received in revised form 2 May 2014
Accepted 10 May 2014
Available online 29 May 2014
Editor: L. Stixrude

Keywords:
Earth's lower mantle
Fe spin crossover
partitioning behavior
oxidation state

ABSTRACT

Geophysical interpretations of the Earth's interior and its dynamics are significantly influenced by phase transitions of the constituting minerals and their chemical compositions. Pressure induced Fe spin crossovers in the main mineral phases of the Earth's lower mantle, Mg–Fe silicate perovskite and ferropericlase, have been suggested to influence Fe partitioning resulting in separate layers with distinct physical properties. However, previous results remain ambiguous regarding the exact effect of Fe spin crossovers and the actual transition pressures. We observe here a continuous decrease of the Fe^{2+}–Mg partition coefficient K_D between silicate perovskite and ferropericlase from 25 GPa to 79 GPa in a pyrolitic Earth's lower mantle system. At about 97 GPa the K_D significantly increases with an accompanied decrease of the $Fe^{3+}/\Sigma Fe$ ratio in perovskite, which therefore leads to an amplified change in the Fe^{2+} K_D. We conclude that the Fe^{2+} high-spin to low-spin crossover in ferropericlase and the Fe^{2+} high-spin to intermediate spin crossover in perovskite at mid-lower mantle pressures (30–80 GPa) exert no control on K_D, but the Fe^{2+} intermediate-spin to low-spin crossover in silicate perovskite at about 100 GPa preferentially partitions Fe into silicate perovskite and reduces its Fe^{3+} content. The change in oxidation state and partitioning behavior of Fe will increase thermal conductivity and probably could induce a thermal boundary layer at this depth.

© 2014 Elsevier B.V. All rights reserved.

1. Introduction

The concentration of iron and its oxidation state in minerals of the Earth's lower mantle are fundamental for understanding the structure and dynamics of the Earth's interior. Both factors significantly influence densities, elasticity, and transport properties such as electrical and thermal conductivities of the major minerals constituting the lower mantle. In comparison to the complex structure of the Earth's upper mantle, the lower mantle is considered to be relatively homogeneous. However, recent seismological studies have demonstrated that discontinuities exist in the upper and lower sections of the lower mantle (Kaneshima and Helffrich, 1999; Kawakatsu and Niu, 1994; Van der Hilst, 1999; Williams and Garnero, 1996). These discontinuities have been attributed either to the presence of remnant subducted slabs (Kaneshima and Helffrich, 1999; Kawakatsu and Niu, 1994), melts (3), or electron spin crossovers in Fe-bearing materials (Badro et al., 2003). To assign these discontinuities to a specific origin, precise investigation of phase relations and partitioning behavior between the minerals constituting the Earth's lower mantle is needed.

In a pyrolitic mantle system, major phases constituting the Earth's lower mantle are Mg-silicate perovskite (Mg–Pv), ferropericlase (Fp) and Ca-silicate perovskite (Ca–Pv). In addition, majorite garnet (Irifune, 1994) and post-perovskite (Murakami et al., 2004) are present in the uppermost and lowermost parts of the lower mantle, respectively. Experimental investigations in simplified MgO–FeO–SiO_2 systems have shown that Fe preferentially partitions into Fp relative to Mg–Pv, with the partitioning coefficient $K_D = (Fe/Mg)_{Mg-Pv}/(Fe/Mg)_{Fp}$ ranging from 0.1–0.3 (Ito and Takahashi, 1989; Nakajima et al., 2012; Narygina et al., 2011; Sakai et al., 2009; Sinmyo et al., 2008). However, in more complex systems, particularly in the presence of Al, the partitioning coefficient K_D increases considerably to about 0.35–0.9 due to the coupled incorporation of Fe^{3+} and Al^{3+} for Mg^{2+} and

* Corresponding author.
E-mail address: clemens.prescher@gmail.com (C. Prescher).
[1] Present address: Center for Advanced Radiation Sources, University of Chicago, Chicago, IL 60439, USA.

http://dx.doi.org/10.1016/j.epsl.2014.05.011
0012-821X/© 2014 Elsevier B.V. All rights reserved.

Si^{4+} in Mg–Pv (Frost and Langenhorst, 2002; Irifune et al., 2010; Kesson et al., 2002; Murakami et al., 2005). Laser heated diamond anvil cell (LHDAC) studies report a K_D of ~0.4–0.5 from 25 to 90 GPa (Kesson et al., 1998; Murakami et al., 2005; Sinmyo and Hirose, 2013) and a subsequent increase to 0.9 at 120 GPa (Sinmyo and Hirose, 2013). However, multi-anvil studies have shown a K_D increasing to almost unity in the top of the lower mantle (30 GPa) with a subsequent drop in K_D at 40 GPa (Irifune et al., 2010) to the values obtained by LHDAC experiments (Kesson et al., 2002; Murakami et al., 2005).

All of the previous investigations on the Fe partitioning behavior in the Earth's lower mantle have reported K_D values for bulk iron content in the constituting minerals, neglecting the oxidation state of iron or used only indirect measures. It is however well known that Fe^{3+} is structurally stabilized in Mg–Pv (Lauterbach et al., 2000; Frost and Langenhorst, 2002). The formation of Fe^{3+} is explained by a disproportionation reaction of the form: $3Fe^{2+} \rightarrow 2Fe^{3+} + Fe^0$ (Frost et al., 2004). This reaction is considered to exert an important control on the partitioning of siderophile elements in the lower mantle. Furthermore, the Fe^{3+} content is a major factor determining the physical properties of Mg–Pv and Fp, such as their elasticities (Glazyrin et al., 2014) and thermal conductivities (Goncharov et al., 2010, 2009). Besides the Fe^{3+} content, electron spin crossovers of Fe in Fp and Mg–Pv have been proposed to significantly alter the K_D in favor of the phase with stable Fe (Badro et al., 2003).

To estimate the effect of spin crossovers on the partitioning behavior and oxidation state of Fe, we have separately determined the Fe^{2+} and Fe^{3+} partitioning coefficients between Mg–Pv and Fp in a pyrolitic lower mantle system at pressure and temperature conditions of the whole Earth's lower mantle.

2. Experimental details

A pyrolitic starting powder was prepared from reagent grade oxides with Fe added as hematite (in wt%, SiO_2: 44.95; TiO_2: 0.71; Al_2O_3: 3.53; FeO: 9.33; MgO: 37.30; CaO: 3.06; Na_2O: 0.57; K_2O: 0.13; Cr_2O_3: 0.43). The oxides were ground together, cold pressed into pellets and then fired in a CO–CO_2 gas mixing furnace at 1000 °C for 1 day at an oxygen fugacity 2 log units below the fayalite magnetite quartz buffer. Quenched samples were re-ground thoroughly. The absence of remnant hematite in the starting powder was confirmed by Mössbauer spectroscopy. The pyrolitic lower mantle assemblage was then synthesized employing a multianvil press with 7/3 octahedral pressure assemblies. A $LaCrO_3$ furnace and a Re capsule were used. The experiment was run for 8 h at 25 GPa and 1650 °C. The recovered sample was crushed and subsequently used as starting material for the diamond anvil cell experiments. A Mössbauer spectrum of the synthesized starting material was recorded at room temperature in transmission mode on a constant acceleration Mössbauer spectrometer with a nominal 370 MBq ^{57}Co high specific activity source in a 12-μm-thick Rh matrix. The velocity scale was calibrated relative to a 25-μm-thick natural α-Fe foil. The spectrum was analyzed with the MossA software package (Prescher et al., 2012).

Six separate laser heated diamond anvil experiments between 33 to 130 GPa were conducted. Ne was used as pressure medium and pressure calibrant (Kurnosov et al., 2008). A double-sided YLF laser system with a Pi-shaper was used for heating the samples to temperatures corresponding to respective geotherm temperatures at each pressure. Each sample was heated for at least 30 min to ensure equilibrium. Detailed experimental conditions are given in Table 1. X-ray diffraction maps of every experiment were measured before and after heating to observe if any phase changes or phase transformations occurred. X-ray diffraction spectra were measured using a monochromatic X-ray beam (0.3344 Å) at 13ID-D of the Advanced Photon Source (APS), Argonne National Laboratory (ANL).

Table 1
Experimental conditions of the laser heated diamond anvil cell experiments. Errors in pressure were calculated by estimating the pressure from the Ne equation of state before and after the heating procedure. Temperatures are calculated as mean values from measured temperatures every minute of the 30 min laser heating time. Errors in temperatures are calculated as standard mean deviation.

Sample	Pressure (GPa)	T (K)	D_C (μm)	D_S (μm)
PyAPS-C6	33(1)	1980(80)	250	120
PyAPS-C4	40(2)	2120(150)	250	120
PyAPS-C5	59(2)	2190(90)	250	120
PyAPS-C2	79(2)	2300(140)	120_B	60_L
PyAPS-C1	97(3)	2450(140)	120_B	60_L
PyAPS-C7	130(3)	2500(150)	60_B	30_L

D_C – diamond anvil culet diameter, B – beveled diamond anvil; D_S – sample hole diameter, L – was drilled by laser.

Thin slices of 30–60 nm thickness were prepared from the central laser heated part of the recovered samples and the starting material using the FEI Quanta3D field-emission FIB-SEM. These slices were observed in a PHILIPS CM20 FEG (field emission gun) STEM operating at 200 kV. To reduce electron irradiation damage during operation, TEM thin foils were cooled to nearly liquid nitrogen temperature (ca. 100 K) in a Gatan cooling holder. Compositions were determined using a ThermoNoran Vantage energy-dispersive X-ray (EDX) microanalysis system equipped with a Norvar ultra-thin window and a germanium detector. The EDX spectra were quantified according to the method by van Cappellen and Doukhan (1994), involving an absorption correction on the basis of charge balance between cations and anions and taking into account the $Fe^{3+}/\Sigma Fe$ ratios determined by electron energy loss spectroscopy (EELS). EDX maps were measured for every recovered sample in order to detect possible chemical heterogeneities. The $Fe^{3+}/\Sigma Fe$ ratios were analyzed using a Gatan PEELS 666 (parallel electron energy-loss spectrometer). The determination of the $Fe^{3+}/\Sigma Fe$ ratio was based on the quantification method of Van Aken and Liebscher (2002). This method is based on the white line intensities at the Fe $L_{2,3}$ edge. Fe $L_{2,3}$ ELNES spectra were measured in diffraction mode with an energy dispersion of 0.01 eV per channel. An energy resolution, measured as width of the zero-loss peak at half maximum, of 0.8–0.9 was obtained. Special care was taken to only measure fresh crystalline grains of magnesium silicate perovskite, since Mg–Pv easily amorphizes under the high electron flux needed for Fe–L edge EELS measurements. To check for possible beam induced changes in valence state, six spectra were measured in a time series with integration times of 20 s each. Spectra were then corrected for dark current and channel-to-channel gain variation. The pure single-scattering core-loss signal was extracted by subtracting an inverse power-law background and removing the multiple scattering contribution by the Fourier-ratio technique (Egerton, 1996). The consistency of the $Fe^{3+}/\Sigma Fe$ ratios estimated from EELS was checked performing EELS and Mössbauer spectroscopy measurements on different Mg–Si perovskites. The resulting $Fe^{3+}/\Sigma Fe$ ratios are in agreement within experimental uncertainties.

3. Results and discussion

The EDX maps of the recovered samples show that the samples are chemically homogeneous (Fig. 1) and do not show any evidence of Soret diffusion. We did not observe strong differences of the chemical compositions of Mg–Pv and Fp in the heated areas, on the contrary to previously reported studies on Mg/Fe partitioning in a pyrolitic system (Sinmyo and Hirose, 2013, 2010). This is probably partly because of the flat-top laser heating system

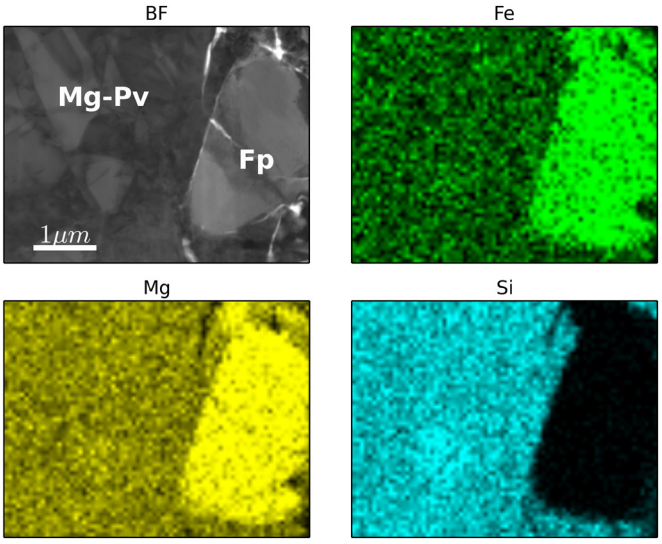

Fig. 1. STEM bright field image (BF) and STEM EDS elemental maps of an interface between Mg–Si perovskite (Mg–Pv) and ferropericlase (Fp) of the sample recovered from the laser heated DAC experiment at 33 GPa and 1980(80) K.

we have employed and partly because we used a pre-synthesized sample. The effort which Sinmyo and Hirose (2013) had to put into minimizing their temperature gradients are directly related to their initial choices for performing the experiments. They used an amorphous gel as a starting material, which could create temperature hotspots due to phase transformations, and they used gold as a laser absorber, which leads to localized heating spots inducing strong temperature gradients.

The concentrations of major elements in Mg–Pv stay almost constant over the entire pressure range investigated (Table 2), whereas the Fe content in Fp increases from 26 GPa to 79 GPa, drops at 97 GPa and increases again at 130 GPa. The resulting bulk Fe K_D is thus largely controlled by the variation of Mg and Fe contents in Fp. The bulk Fe K_D linearly decreases from 0.58 at 26 GPa to 0.45 at 79 GPa, then abruptly increases to 0.57 at 97 GPa and decreases again to 0.48 at 130 GPa (Fig. 2A). The $Fe^{3+}/\Sigma Fe$ ratio in Mg–Pv is 42(5)% in the starting material and stays almost constant up to 79 GPa; at 97 GPa it drops to ~30% (Fig. 3A, D). On the contrary, the $Fe^{3+}/\Sigma Fe$ ratio of Fp increases from under 5% in the starting material to about 16% at 59 GPa and stays constant up to 130 GPa (Fig. 3B, D). By combining bulk Fe K_D and the $Fe^{3+}/\Sigma Fe$ ratios we can estimate the partitioning coefficient of Fe^{2+} and Fe^{3+} separately (Fig. 2B). The Fe^{3+} partitioning coefficient decreases in the investigated pressure range and reaches almost unity at 130 GPa, whereas the Fe^{2+} partitioning coefficient first deceases linearly up to 79 GPa from 0.4 to 0.22, jumps to 0.57 at 97 GPa and decreases again at 130 GPa (Fig. 2B).

In the last decade, it has been demonstrated by experimental and theoretical studies that an electronic high-spin (HS) to low-spin (LS) crossover of Fe^{2+} occurs in Fp over a large pressure range from ~35 GPa to 80 GPa (Badro et al., 2003; Lin et al., 2007, 2005). The effective ionic radius of Fe^{2+} in LS state is smaller than that of Mg^{2+}, which should significantly alter the partitioning behavior. Recently, this spin crossover has been proposed to induce a discontinuity in bulk Fe K_D in a pyrolitic composition at ~40 GPa (Irifune et al., 2010). However, our results and previous estimates (Kesson et al., 1998; Murakami et al., 2005; Sinmyo and Hirose, 2013) lack abrupt changes at this pressure and show a rather smooth decrease of K_D, which is a reasonable behavior considering the broad pressure range of the spin crossover. Two other studies using San Carlos olivine with a composition of $(Mg_{0.9}Fe_{0.1})SiO_4$ as starting material proposed a gradual decrease in K_D above pressures of ~70 GPa (Auzende et al., 2008; Sakai et al., 2009). On the contrary, a careful examination of chemical heterogeneity using the same starting material and LHDAC technique actually shows an increase of K_D in this pressure range (Sinmyo et al., 2008). Thus, it is unclear whether the Fe^{2+} spin crossover in Fp really affects the K_D in an olivine system or whether variations can be explained by experimental uncertainties. In case of pyrolitic composition reported so far data suggest that the spin crossover in Fp does not have a pronounced effect on K_D (Fig. 2, see also Murakami et al., 2005).

Electronic spin crossovers of Fe have also been reported for Mg–Pv but data on the spin crossover pressures do not give a uniform picture. Some authors propose an onset of a Fe^{2+} HS to intermediate-spin (IS) crossover at about 35 GPa (McCammon et al., 2008), whereas others suggest that Fe^{2+} and Fe^{3+} occupying the bicapped trigonal prism ("A") crystallographic site stay in HS state, and only Fe^{3+} occupying the octahedral ("B") site undergoes HS to LS crossover at 40–60 GPa (Catalli et al., 2010). Additionally, it has been shown that Fe^{2+} becomes LS in Mg–Pv at about 110 GPa at high temperature (McCammon et al., 2010). The ionic radii of HS and IS Fe^{2+} are similar, whereby there is a decrease in electronic entropy which may lower the K_D at the HS–IS crossover. However, the IS-LS crossover occurs over a large pressure range (McCammon et al., 2008) and overlaps with the HS–LS crossover in Fp which makes it difficult to assign the smooth decrease of K_D

Table 2
Element composition of Fp calculated per 1 oxygen and element composition of Mg–Pv calculated per 3 oxygens with its ferric iron contents (%).

Pressure (GPa)	Fp					
	Mg	Fe	$Fe^{3+}/\Sigma Fe$	Cr	Al	Na
26(2)	0.800(5)	0.158(4)	n.d.	0.0065(6)	0.0015(9)	0.027(2)
33(1)	0.82(3)	0.16(2)	5(5)	0.004(3)	0.004(4)	0.027(8)
40(2)	0.83(2)	0.15(1)	9(5)	n.d.	0.005(2)	0.023(7)
59(2)	0.80(3)	0.17(3)	17(5)	n.d.	n.d.	0.02(1)
79(2)	0.77(1)	0.19(1)	16(5)	n.d.	0.01(5)	n.d.
97(3)	0.79(1)	0.155(3)	n.d.	0.006(1)	0.001(1)	0.027(2)
130(3)	0.78(1)	0.167(4)	14(5)	0.008(1)	0.004(4)	0.018(8)

	Mg–Pv							
	Mg	Fe	$Fe^{3+}/\Sigma Fe$	Ca	Cr	Al	Si	Ti
26(2)	0.85(1)	0.098(2)	42(3)	0.019(5)	0.0036(6)	0.05(1)	0.957(6)	0.0087(8)
33(1)	0.85(2)	0.101(6)	44(7)	0.019(2)	n.d.	0.066(27)	0.95(2)	0.0102(14)
40(2)	0.89(3)	0.091(3)	39(7)	0.011(9)	n.d.	0.054(4)	0.955(6)	n.d.
59(2)	0.88(2)	0.095(10)	49(7)	0.016(3)	n.d.	0.058(5)	0.95(1)	n.d.
79(2)	0.87(1)	0.097(3)	50(7)	0.017(3)	n.d.	0.058(3)	0.95(1)	n.d.
97(3)	0.86(1)	0.096(3)	31(7)	0.019(4)	0.0033(7)	0.043(3)	0.96(1)	0.008(1)
130(3)	0.87(1)	0.090(9)	31(7)	0.017(2)	0.0038(6)	0.045(5)	0.96(1)	0.009(1)

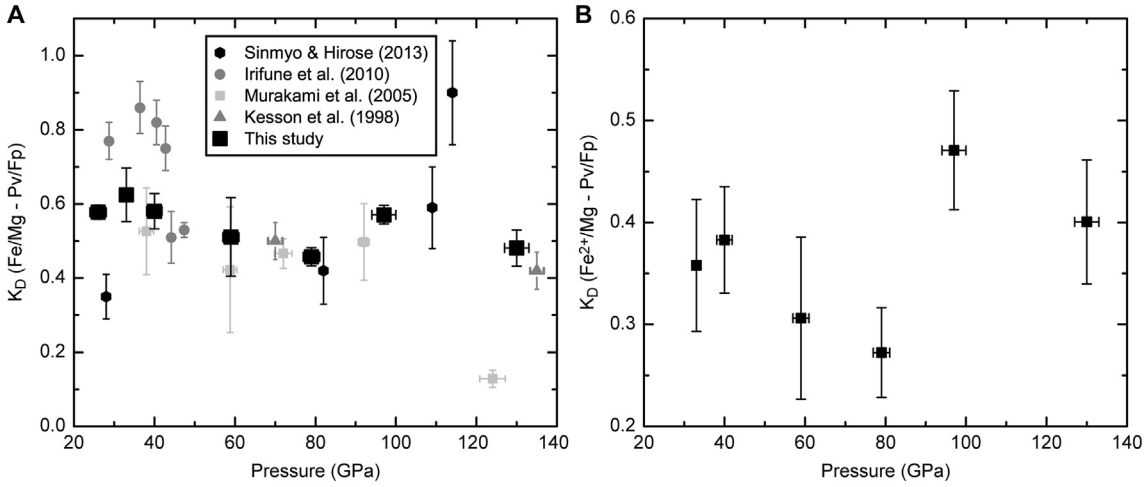

Fig. 2. **A** Variations of the Fe–Mg K_D between Mg–Pv and Fp in pyrolite as a function of pressure. Data is compared with previous studies on a pyrolitic lower mantle assemblage. **B** Calculated Fe^{2+}–Mg K_D between Mg–Pv and Fp in pyrolite on the basis of the bulk Fe K_D and $Fe^{3+}/\Sigma Fe$ ratios estimated. The Fp $Fe^{3+}/\Sigma Fe$ ratio at 97 GPa has been estimated by linear interpolation between the adjacent points. The pressure evolution shows a discontinuity at about 100 GPa probably produced by the IS–LS crossover of Fe^{2+} in Mg–Pv.

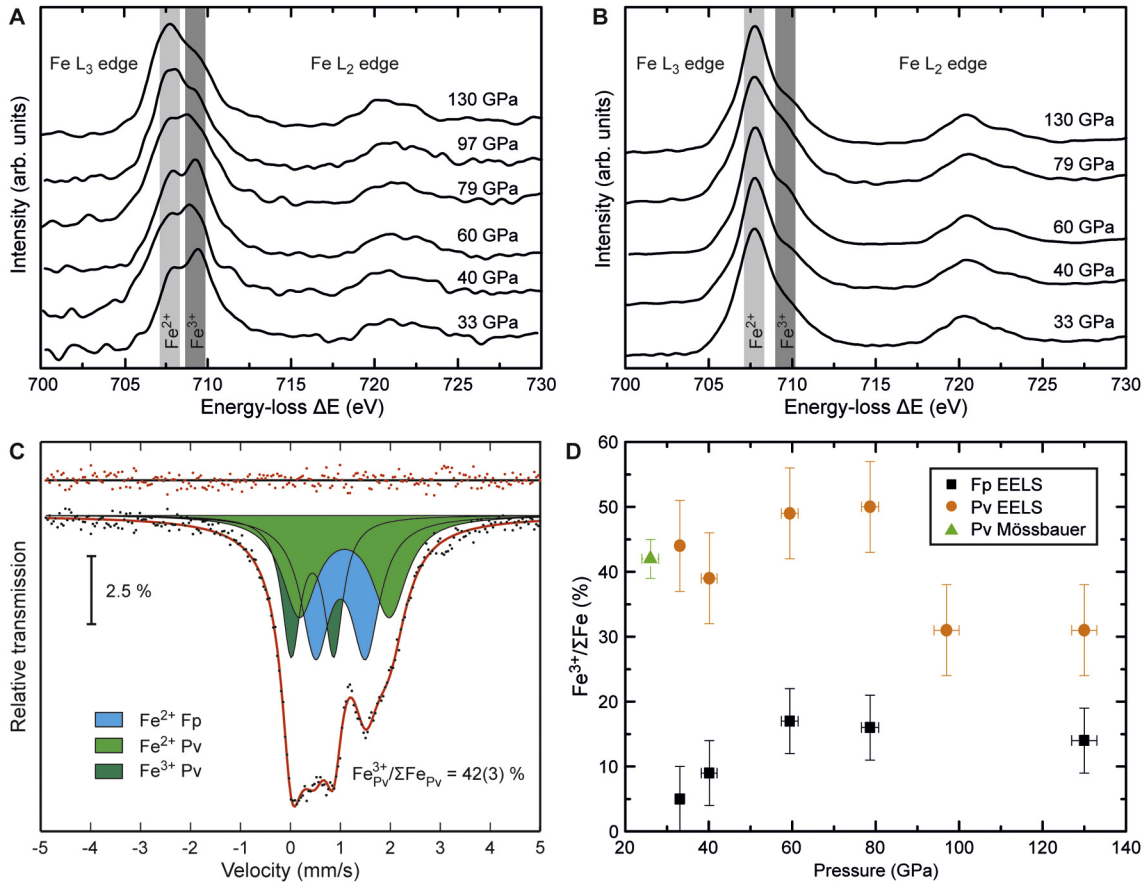

Fig. 3. Respective Fe $L_{2,3}$ electron energy loss spectra (EELS) of **A** Mg–Pv and **B** Fp at each pressure point. **C** Mössbauer spectrum of the pyrolitic starting material synthesized in a multianvil apparatus. **D** Variation in $Fe^{3+}/\Sigma Fe$ ratio of Mg–Pv and Fp in pyrolitic lower mantle system with pressure and the respective geotherm temperatures.

to either spin crossovers. Nevertheless, a relatively narrow Fe^{2+} IS to LS crossover would result in a preferential partitioning of Fe^{2+} into Mg–Pv due to a change in atomic radii being shown by an increase in K_D. This is exactly what can be seen in the behavior of the bulk and Fe^{2+} K_D at ~100 GPa (Fig. 2).

Sinmyo and Hirose (2013) suggested that their observed increase of K_D from 0.42(9) at 82 GPa to 0.90(14) at 114 GPa is caused by the HS–LS crossover in Fe^{3+} occupying the B-site of the Mg–Pv structure, based on a slight increase of the $Fe^{3+}/\Sigma Fe$ ratio from 0.50(9) to 0.59(12), whereby those values were either inferred indirectly or measured from an amorphized recovered sample. However, such a strong effect on K_D due to the spin crossover of a small amount of Fe^{3+} on the B-site is implausible. Our measurements on recovered crystalline Mg–Pv oppose this hypothesis and show that the Fe^{3+}content of Mg–Pv rather decreases than increases. Additionally, our data lacks evidence for Fe^{3+} occupying

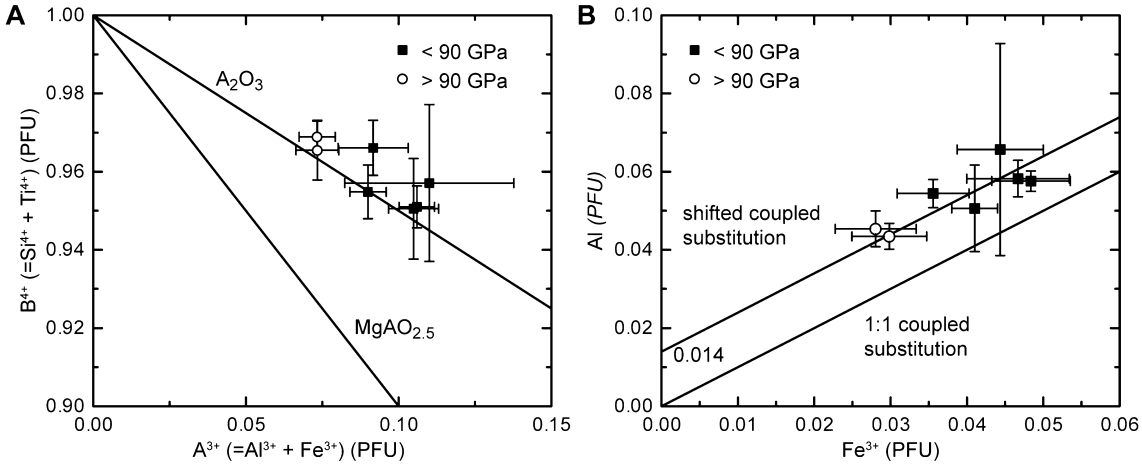

Fig. 4. A Plot of the 4-valent cations (Si^{4+} and Ti^{4+}) against the 3-valent cations (Al^{3+} and Fe^{3+}) per formula unit (PFU) in Mg–Pv. The lines indicate two possible substitution mechanisms, the A_2O_3 substitution indicates that the incorporation of A^{3+} cations takes place onto both six-fold and eight-fold sites (coupled substitution), while the $MgAO_{2.5}$ substitution indicates that A^{3+} cations are only incorporated on the six-fold site and the charge is balanced by oxygen vacancies. **B** Plot of Al^{3+} against Fe^{3+} content per formula unit (PFU) in Mg–Pv showing that all Fe^{3+} is charge balanced by Al through a $Fe^{3+}AlO_3$ component. The shift of the 1:1 lines indicates that an Al_2O_3 component is also present with an abundance determined by the y-axis intersection (0.014). Both plots show that the mechanism of Fe^{3+} incorporation is not affected by the increase of the Fe^{2+} K_D and the decrease of the $Fe^{3+}/\Sigma Fe$ ratio in Mg–Pv above 90 GPa.

the B-site of Mg–Pv (Fig. 4), supporting a recent single crystal X-ray diffraction study (Glazyrin et al., 2014), which has shown that within experimental uncertainty (about 5% of total iron) Fe only occupies the A site in Al bearing Mg–Pv. The only plausible explanation for the decrease in $Fe^{3+}/\Sigma Fe$ in Mg–Pv ratio with an accompanied increase in Fe^{2+} K_D observed in the present study is the Fe^{2+} IS–LS crossover in Mg–Pv.

The discontinuous change in bulk K_D is mainly caused by a decrease in Fe content in Fp and is accompanied by a relative decrease of the Fe^{3+} content in Mg–Pv, whereby the bulk Fe concentration in Mg–Pv remains the same, resulting in an amplified increase in the Fe^{2+} K_D (Fig. 2). On the basis of the change in K_D and the change in Fe^{3+} in Pv at 97 GPa we propose that the electronic IS–LS crossover of Fe^{2+} not only affects the partitioning behavior of Fe^{2+}, it also may cause a self-reduction of Fe^{3+} to Fe^{2+} in Mg–Pv. Experimental investigations of the $Fe^{3+}/\Sigma Fe$ ratio in Al-bearing Mg–Pv at low pressures have shown that the Fe^{3+} content is mainly controlled by the Al content due to the coupled substitution of (Mg^{2+}, Fe^{2+})–Si^{4+} with Fe^{3+}–Al^{3+} (Frost and Langenhorst, 2002; Lauterbach et al., 2000). Due to the Fe^{2+} IS–LS crossover this relationship is eventually reversed at high pressures. The coupled substitution mechanism is still dominant, but the self-reduction of Fe^{3+} to Fe^{2+} results in a decreasing Al content (Fig. 4). The Al content of Ca–Pv and Fp stays constant at this pressure; therefore it is unclear where the excessive Al remains. A possibility would be the formation of a small amount of an Al-rich phase, although we did not see any direct evidence for the presence of the additional phase either in-situ by X-ray diffraction or in the TEM.

The reduction of Fe^{3+} to Fe^{2+} needs to be balanced by oxidation of some other components. Diamond or volatile species such as CH_4 or H_2 could be oxidized to form CO_2 or H_2O. In the DAC experiments probably the diamond anvils were the reaction partner; however, the budget of those components in the Earth's lower mantle is too low (probably on the order of 2000 ppm, Wood et al., 1996) to account for the reduction alone. A more realistic scenario for the Earth would be that the amount of metallic Fe by disproportionation of Fe^{2+} (Frost et al., 2004) during crystallization of an early magma ocean is reduced at this depth.

Another important effect of the change in Fe^{3+} content of Mg–Pv is the induced change in thermal conductivity. It has been shown that the radiative contribution of the thermal conductivity in Mg–Pv mainly depends on its Fe^{3+} content due to Fe^{2+}–Fe^{3+} and Fe^{3+}–O^{2-} charge transfer bands (Goncharov et al., 2010, 2009). A decrease of Fe^{3+} content at 97 GPa will increase the thermal conductivity, creating a discontinuity, which could act as thermal boundary layer between the mid-lower mantle and the lowermost lower mantle.

Acknowledgements

We thank C.M. McCammon for providing help in the Mössbauer laboratory and G. Manthilake for giving support during the multi-anvil experiments. We also acknowledge financial support provided by the Deutsche Forschungsgemeinschaft (LA 830/14-1 to F.L.). Portions of this work were performed at GeoSoilEnviroCARS (Sector 13), Advanced Photon Source (APS), Argonne National Laboratory. GeoSoilEnviroCARS is supported by the National Science Foundation – Earth Sciences (EAR-1128799) and Department of Energy – Geosciences (DE-FG02-94ER14466). Use of the Advanced Photon Source was supported by the U.S. Department of Energy, Office of Science, Office of Basic Energy Sciences, under Contract No. DE-AC02-06CH11357.

References

Auzende, A.-L., Badro, J., Ryerson, F.J., Weber, P.K., Fallon, S.J., Addad, A., Siebert, J., Fiquet, G., 2008. Element partitioning between magnesium silicate perovskite and ferropericlase: new insights into bulk lower-mantle geochemistry. Earth Planet. Sci. Lett. 269, 164–174. http://dx.doi.org/10.1016/j.epsl.2008.02.001.

Badro, J., Fiquet, G., Guyot, F., Rueff, J.-P., Struzhkin, V.V., Vankó, G., Monaco, G., 2003. Iron partitioning in Earth's mantle: toward a deep lower mantle discontinuity. Science 300, 789–791. http://dx.doi.org/10.1126/science.1081311.

Catalli, K., Shim, S.-H., Prakapenka, V.B., Zhao, J., Sturhahn, W., Chow, P., Xiao, Y., Liu, H., Cynn, H., Evans, W.J., 2010. Spin state of ferric iron in $MgSiO_3$ perovskite and its effect on elastic properties. Earth Planet. Sci. Lett. 289, 68–75. http://dx.doi.org/10.1016/j.epsl.2009.10.029.

Egerton, R.F., 1996. Electron Energy Loss Spectroscopy in the Electron Microscope, 2nd ed. Springer, New York.

Frost, D.J., Langenhorst, F., 2002. The effect of Al_2O_3 on Fe–Mg partitioning between magnesiowüstite and magnesium silicate perovskite. Earth Planet. Sci. Lett. 199.

Frost, D.J., Liebske, C., Langenhorst, F., McCammon, C.A., Tronnes, R.G., Rubie, D.C., 2004. Experimental evidence for the existence of iron-rich metal in the Earth's lower mantle. Nature 428, 409–412. http://dx.doi.org/10.1029/200/JC000964.

Glazyrin, K., Boffa Ballaran, T., Frost, D.J., McCammon, C., Kantor, A., Merlini, M., Hanfland, M., Dubrovinsky, L., 2014. Magnesium silicate perovskite and effect of iron oxidation state on its bulk sound velocity at the conditions of the lower mantle. Earth Planet. Sci. Lett. 393, 182–186. http://dx.doi.org/10.1016/j.epsl.2014.01.056.

Goncharov, A.F., Beck, P., Struzhkin, V.V., Haugen, B.D., Jacobsen, S.D., 2009. Thermal conductivity of lower-mantle minerals. Phys. Earth Planet. Inter. 174, 24–32. http://dx.doi.org/10.1016/j.pepi.2008.07.033.

Goncharov, A.F., Struzhkin, V.V., Montoya, J.A., Kharlamova, S., Kundargi, R., Siebert, J., Badro, J., Antonangeli, D., Ryerson, F.J., Mao, W., 2010. Effect of composition, structure, and spin state on the thermal conductivity of the Earth's lower mantle. Phys. Earth Planet. Inter. 180, 148–153. http://dx.doi.org/10.1016/j.pepi.2010.02.002.

Irifune, T., 1994. Absence of an aluminous phase in the upper part of the Earth's lower mantle. Nature 370, 131–133.

Irifune, T., Shinmei, T., McCammon, C.A., Miyajima, N., Rubie, D.C., Frost, D.J., 2010. Iron partitioning and density changes of pyrolite in Earth's lower mantle. Science 327, 193–195. http://dx.doi.org/10.1126/science.1181443.

Ito, E., Takahashi, E., 1989. Postspinel transformations in the system Mg_2SiO_4–Fe_2SiO_4 and some geophysical implications. J. Geophys. Res. 94, 10637–10646. http://dx.doi.org/10.1029/JB094iB08p10637.

Kaneshima, S., Helffrich, G., 1999. Dipping low-velocity layer in the mid-lower mantle: evidence for geochemical heterogeneity. Science 283, 1888–1892. http://dx.doi.org/10.1126/science.283.5409.1888.

Kawakatsu, H., Niu, F., 1994. Seismic evidence for a 920-km discontinuity in the mantle. Nature 371, 301–305.

Kesson, S.E., Fitz Gerald, J.D., Shelley, J.M., 1998. Mineralogy and dynamics of a pyrolite lower mantle. Nature 393, 3–6.

Kesson, S., Gerald, J.D.F., O'Neill, H.S.C., Shelley, J.M.G., 2002. Partitioning of iron between magnesian silicate perovskite and magnesiowüstite at about 1 Mbar. Phys. Earth Planet. Inter. 131, 295–310. http://dx.doi.org/10.1016/S0031-9201(02)00063-8.

Kurnosov, A., Kantor, I., Boffa-Ballaran, T., Lindhardt, S., Dubrovinsky, L., Kuznetsov, A., Zehnder, B.H., 2008. A novel gas-loading system for mechanically closing of various types of diamond anvil cells. Rev. Sci. Instrum. 79. http://dx.doi.org/10.1063/1.2902506. 045110.

Lauterbach, S., McCammon, C.A., van Aken, P., Langenhorst, F., Seifert, F., 2000. Mössbauer and ELNES spectroscopy of (Mg, Fe)(Si, Al)O_3 perovskite: a highly oxidised component of the lower mantle. Contrib. Mineral. Petrol., 17–26.

Lin, J.-F., Struzhkin, V.V., Jacobsen, S.D., Hu, M.Y., Chow, P., Kung, J., Liu, H., Mao, H.-K., Hemley, R.J., 2005. Spin transition of iron in magnesiowüstite in the Earth's lower mantle. Nature 436, 377–380. http://dx.doi.org/10.1038/nature03825.

Lin, J.-F., Vankó, G., Jacobsen, S.D., Iota, V., Struzhkin, V.V., Prakapenka, V.B., Kuznetsov, A., Yoo, C.-S., 2007. Spin transition zone in Earth's lower mantle. Science 317, 1740–1743. http://dx.doi.org/10.1126/science.1144997.

McCammon, C., Kantor, I., Narygina, O., Rouquette, J., Ponkratz, U., Sergueev, I., Mezouar, M., Prakapenka, V., Dubrovinsky, L., 2008. Stable intermediate-spin ferrous iron in lower-mantle perovskite. Nat. Geosci. 1, 684–687. http://dx.doi.org/10.1038/ngeo309.

McCammon, C., Dubrovinsky, L., Narygina, O., Kantor, I., Wu, X., Glazyrin, K., Sergueev, I., Chumakov, A.I., 2010. Low-spin Fe^{2+} in silicate perovskite and a possible layer at the base of the lower mantle. Phys. Earth Planet. Inter. 180, 215–221. http://dx.doi.org/10.1016/j.pepi.2009.10.012.

Murakami, M., Hirose, K., Kawamura, K., Sata, N., Ohishi, Y., 2004. Post-perovskite phase transition in $MgSiO_3$. Science 304, 855–858. http://dx.doi.org/10.1126/science.1095932.

Murakami, M., Hirose, K., Sata, N., Ohishi, Y., 2005. Post-perovskite phase transition and mineral chemistry in the pyrolitic lowermost mantle. Geophys. Res. Lett. 32. http://dx.doi.org/10.1029/2004GL021956. L03304.

Nakajima, Y., Frost, D.J., Rubie, D.C., 2012. Ferrous iron partitioning between magnesium silicate perovskite and ferropericlase and the composition of perovskite in the Earth's lower mantle. J. Geophys. Res. 117, 1–12. http://dx.doi.org/10.1029/2012JB009151.

Narygina, O., Dubrovinsky, L.S., Samuel, H., McCammon, C.A., Kantor, I.Y., Glazyrin, K., Pascarelli, S., Aquilanti, G., Prakapenka, V.B., 2011. Chemically homogeneous spin transition zone in Earth's lower mantle. Phys. Earth Planet. Inter. 185, 107–111. http://dx.doi.org/10.1016/j.pepi.2011.02.004.

Prescher, C., McCammon, C., Dubrovinsky, L., 2012. MossA: a program for analyzing energy-domain Mössbauer spectra from conventional and synchrotron sources. J. Appl. Crystallogr. 45, 329–331. http://dx.doi.org/10.1107/S0021889812004979.

Sakai, T., Ohtani, E., Terasaki, H., Sawada, N., Kobayashi, Y., Miyahara, M., Nishijima, M., Hirao, N., Ohishi, Y., Kikegawa, T., 2009. Fe–Mg partitioning between perovskite and ferropericlase in the lower mantle. Am. Mineral. 94, 921–925. http://dx.doi.org/10.2138/am.2009.3123.

Sinmyo, R., Hirose, K., 2010. The Soret diffusion in laser-heated diamond-anvil cell. Phys. Earth Planet. Inter. 180, 172–178. http://dx.doi.org/10.1016/j.pepi.2009.10.011.

Sinmyo, R., Hirose, K., 2013. Iron partitioning in pyrolitic lower mantle. Phys. Chem. Miner. 40, 107–113. http://dx.doi.org/10.1007/s00269-012-0551-7.

Sinmyo, R., Hirose, K., Nishio-Hamane, D., Seto, Y., Fujino, K., Sata, N., Ohishi, Y., 2008. Partitioning of iron between perovskite/postperovskite and ferropericlase in the lower mantle. J. Geophys. Res. 113, 1–11. http://dx.doi.org/10.1029/2008JB005730.

Van Aken, P.A., Liebscher, B., 2002. Quantification of ferrous/ferric ratios in minerals: new evaluation schemes of Fe L 23 electron energy-loss near-edge spectra. Phys. Chem. Miner. 29, 188–200. http://dx.doi.org/10.1007/s00269-001-0222-6.

Van Cappellen, E., Doukhan, J.C., 1994. Quantitative transmission X-ray microanalysis of ionic compounds. Ultramicroscopy 53, 343–349.

Van der Hilst, R.D., 1999. Compositional heterogeneity in the bottom 1000 kilometers of Earth's mantle: toward a hybrid convection model. Science 283, 1885–1888. http://dx.doi.org/10.1126/science.283.5409.1885.

Williams, Q., Garnero, E.J., 1996. Seismic evidence for partial melt at the base of Earth's mantle. Science 273, 1528–1530. http://dx.doi.org/10.1126/science.273.5281.1528.

Wood, B.J., Pawley, A., Frost, D.R., 1996. Water and carbon in the Earth's mantle. Philos. Trans. R. Soc., Math. Phys. Eng. Sci. 354, 1495–1511. http://dx.doi.org/10.1098/rsta.1996.0060.